Spatiotemporal changes in atmospheric water vapor content and analysis of meteorological factors over the Tibetan Plateau and its surroundings

Zhilan Wang
Northwest Normal University
Meiping Sun (sunmeiping1982@163.com)
Northwest Normal University
Xiaojun Yao
Northwest Normal University
Lei Zhang
Northwest Normal University
Hao Zhang
Northwest Normal University

Research Article

Keywords: Tibetan Plateau and surroundings, Water vapor content, Precipitation, Temperature

Posted Date: March 4th, 2021

DOI: https://doi.org/10.21203/rs.3.rs-271320/v1

Abstract

Based on radiosonde stations and V3.0 data, Atmospheric Infrared Sounder (AIRS)-only, Tropical Rainfall Measuring Mission satellite (TRMM) and MERRA2, and ERA-5 data, we evaluated the ability of each dataset to reproduce water vapor content and explored its relationship with precipitation and temperature over the Tibetan Plateau and its surroundings. The results showed that the southern part of the surrounding area had high water vapor content and a low water vapor content zone appeared in the inner part of the Tibetan Plateau. The largest water vapor content appeared in summer and the smallest in winter. Most of the products could capture the spatial distribution of water vapor content, ERA-5 had the smallest bias and the highest correlation coefficient with the radiosonde data. The water vapor content has shown a gradually increasing trend over the last 50 years, with the most obvious increase in summer. Several sets of products had the same fluctuation trend and value is greater than the radiosonde data. There was a significant positive correlation between air temperature and water vapor content in the Tibetan Plateau, especially in the south. As the latitude increased, the correlation between precipitation and water vapor content gradually decreased and a negative correlation appeared.

Introduction

Atmospheric water vapor is one of the most important hydrological cycle parameters, It is affected by surface-atmosphere energy exchange, and climate change[1]. Water vapor content accounts for only a small proportion of the atmosphere at 0.1–3 %, but it is the most active element of atmospheric circulation and the Earth's climate system[2–4]. The most direct effect of global warming is increasing the amount of water vapor in the air. Air can hold more water vapor as the temperature increase. Studies have shown that for every 1°C increase in temperature, the air will be able to hold 7% more water vapor. Precipitation is a complex process in which the atmosphere collects, lifts, and condenses water vapor in the lower troposphere over the rainfall zone through horizontal transport and dynamic uplift. Therefore, there is a close relationship between temperature, precipitation, and water vapor content. Water vapor transport is an important factor influencing the basic distribution characteristics and trends of regional water resources[4].

The current understanding of water vapor content depends on the evaluation of the "data set" of the Tibetan Plateau (TP) and its surroundings because of the environmental challenges and because the distribution of observation stations is scarce and uneven. Many scholars have calculated and analyzed the relationship between water vapor content distribution and precipitation using different data sources and methods[5–8]. Chen *et al.*[9] combined three sets of reanalysis data from ERA-5, MERRA, and NCEP/NCAR to study the interannual variability of atmospheric water vapor content in summer on the TP. They found that the trend of water vapor content trend on the TP was more similar to ERA-5 and MERRA data than NCEP/NCAR data. Zhang *et al.*[10] found that water vapor on the TP had significant seasonal variations, with more water vapor in the warm season than in the cool season. Zhuo *et al.*[11] concluded that water vapor on the TP decreases from southeast to northwest. Lin *et al.*[12] and Han *et al.*[13] showed

that the seasonal characteristics of precipitation in the plateau had the most precipitation in summer. Yao *et al.*[14] found that the water vapor content in the Tian Shan mountain range showed an increasing trend over the past 50 years, with a single-peak annual distribution. The highest trend was observed in summer, and the lowest was in winter, and there were a significant increase in summer and autumn. However water vapor and precipitation did not correspond well. Zhou *et al.*[15] studied the relationship between water vapor content and precipitation in the TP and found that the summer water vapor content appeared to be higher in the south and lower in the north. There was generally more precipitation in the southern part of the TP and less precipitation in the northern part. Cess[16] and Xie[17] concluded that there is a positive feedback effect between air temperature and water vapor content on the TP. Li *et al.*[18] studied the relationship between atmospheric water vapor content and temperature and precipitation in Changchun, and found that water vapor content had a significant correlation with temperature, while the trend and amplitude of precipitation and water vapor content variation were not consistent. Yao *et al.*[19] found that the changes of precipitation and surface temperature in TP were consistent, which was consistent with the theory of positive feedback effects between temperature and precipitation. The above studies on water vapor content in the atmosphere of the Plateau were mainly based on the results of various reanalysis data, and the reliability of these studies remains to be verified. Meanwhile, few studies have analyzed water vapor content over the Plateau based on multi-source data, and few studies have further analyzed the relationship between water vapor content and surface precipitation and temperature. Thus, this paper studying the distribution characteristics of atmospheric water vapor content and the relationship between precipitation and temperature over the Tibetan Plateau and its surrounding areas, to lays a certain foundation for revealing the changing process of atmospheric water cycle over the Plateau.

Based on data from 27 radiosonde stations, we assessed the quality of Atmospheric Infrared Sounder (AIRS)-only satellite data, ERA-5 and MERRA2 reanalysis data. Weight ensemble data was calculated using the weighted average method. First, the temporal and spatial variation of water vapor content on the TP and surrounding areas were analyzed. The correlation coefficient, bias, and root-mean-square (RMSE) of AIRS-only, MERRA2, ERA-5, and weighted ensemble data were calculated to verify the reliability of the three sets of data in the TP and its surroundings. Finally, the relationship between temperature, precipitation, and water vapor content was analyzed based on Tropical Rainfall Measuring Mission satellite (TRMM), V3.0 precipitation data and ERA-5 temperature data. The seasons in this paper were divided into spring (March–May), summer (June–August), autumn (September–November), and winter (December–February).

Material And Methods

Overview of the study area

The TP and its surroundings are located in the central arid and semi-arid zone of Asia and Europe, as shown in Fig. 1. The region consists of more than 20 mountains ranging from the Pamir and Hindu Kush area in the west to the Hengduan Mountains in the east and from the Altai Mountains in the north to the

Himalayas in the south[20]. This area contains the most dense distribution of glaciers in the world outside of the two polar regions and is the source of 12 important rivers in Asia. Due to differences in latitude, geographic conditions, and circulation forms, the TP and its surroundings have different moisture sources, with the west and north mainly influenced by westerly circulation, the southwest by the strong South Asian monsoon, and the east and southeast by the East Asian monsoon[21]. The TP as the third largest cryosphere in the world[22], and the study of the water vapor content over it and its relationship with precipitation are important for understanding the formation and change of the cryosphere as well as the cyclical effects of the climate system.

Data

Measured data from radiosonde stations

The water vapor content during the period of 1970–2013 was calculated by radiosonde data from the CMSDC There were 88 radiosonde stations in this dataset, comprising 7 different altitude fields. We finally selected 27 stations. As shown in Fig. 1, these stations were mainly located in the eastern part of the TP and surrounding areas. These data have been extensively used in studies on climate change[23, 24], which were be used as a reference to assess the ability of satellite and reanalysis data to capture water vapor content on the TP and surrounding areas.

Satellite data: AIRS-only and TRMM

The Atmospheric Infrared Sounder (AIRS) is one of the instruments aboard the Aqua satellite, provided by NASA as part of the Earth Observation System (EOS) [25]. This paper used monthly water vapor content data from AIRS-onlyversion 6 Level 3 (gridded) [26]. TRMM is a joint mission of NASA and the Japan Aerospace Exploration Agency (JAXA) [27]. The paper used this satellite precipitation data to calculate precipitation for the TP and surrounding areas.

Reanalysis data: ERA-5 and MERRA2

Reanalysis data has been widely used in climate research. Using an assimilation system consistent with the observed data, reanalysis data can effectively reduce errors due to changes in models or analytical methods[28]. In this paper, two reanalysis datasets, ERA-5 and MERRA2, were selected. The ERA-5 data covered the period from1979 to the present[29]. We downloaded the ERA-5 temperature and water vapor content data. MERRA2 is an atmospheric reanalysis product issued by NASA from 1980 onwards[30]. Water vapor content data was used in this article.

Dataset of daily values of terrestrial climate information for China (V3.0)

This paper calculated the annual and seasonal precipitation on the TP and surrounding areas using the m 157 stations from 1970 to 2019. After quality control, the

data became more complete and the quality was significantly improved compared with similar data products released on the ground in the past. More details about the data are shown in Table 1.

Methodology

Water vapor content (*W*, in mm) refers to the mass of water vapor in an atmospheric column of any unit area, also known as atmospheric precipitation water. It means the depth of the water layer formed at the bottom of the atmospheric column after all the water vapor in the column has condensed and landed[31]. It combines relative humidity (q, in kg.kg-1). *Pt* is the pressure at the top of the atmosphere, *Ps* is the pressure near the ground (hPa), and *g* is the acceleration due to gravity (m·s-2).

$$W = \frac{1}{g}\int_{P_s}^{P_t} \mathrm{q}\, dp$$

1

where

$$q = 0.622 \times \frac{e}{P}$$

2

$$e = E_0 \times 10^{\frac{7.45 T_d}{2.35 + T_d}}$$

3

$$T_\mathrm{d} = t - \Delta t$$

4

P is the air pressure (hPa), *e* is the water vapor pressure (hPa), E_0 is the saturated water vapor pressure at 0°C (6.11 hPa), *t* is the temperature of the air at a certain altitude (°C), Δt is the temperature dew point difference (°C), and T_d is the dew point temperature (°C).

Table 1
Information about the data

	Source	Time range	Horizontal resolution
AIRS-only	NASA	2003–2017	1°×1°
MERRA2	NASA	1980–2019	0.5°×0.625°
ERA-5	ECMWF	1980–2019	0.75°×0.75°
Radiosonde	CMSDC	1980–2013	data from 27 stations
V3.0	CMSDC	1970–2019	data from 157 stations
TRMM	NASA	1998–2019	0.25°×0.25°

Results

Product accuracy evaluation

The correlation coefficient, bias, and root mean squared errors (RMSE) between data from each product and radiosonde data on interannual and seasonal scales were calculated in order to evaluate the ability of each product to capture the water vapor content of the TP and its surroundings. The results are shown in Table 2. The error values were used to assign weights to the three sets of data to obtain the weighted ensemble data.

On an annual scale, the correlation was higher than 0.94, and correlation between the reanalysis data and the weighted ensemble data was higher than the satellite data. The highest correlation was the ERA-5 data (0.97). The bias of AIRS-only and ERA-5 data was negative, indicating that the distribution of annual average water vapor content in TP and surrounding areas was underestimated. In contrast, the MERRA2 data appeared to be an overestimation. The weighted ensemble data also had a negative bias, but the difference was significantly smaller (− 0.01). The AIRS-only data had the largest RMSE (2.38). This indicated that the ERA-5, MERRA2, and AIRS-only data had better correlation with the radiosonde data, and the ERA-5 data was the best.

The correlation between each product in different seasons and the radiosonde stations in descending order was winter, spring, autumn and summer. Except for AIRS-only (0.88) in summer, the correlation coefficients of all products were above 0.93. Overall, the highest correlation was ERA-5. In terms of seasonal bias, except for the minimum bias of AIRS-only (0.02 mm) in the spring, the other seasons had the minimum bias using MERRA2, 0.05 mm in summer, 0.02 mm in autumn, and − 0.01 mm in winter. In terms of minimum RMSE, MERRA2 (1.60 mm) was the smallest in spring and the other seasons had the smallest values for ERA-5, 3.06 mm in summer, 2.04 mm in autumn, and 0.97 mm in winter. The RMSE for each product was smaller in winter compared to other seasons. The weighted ensemble data showed

better fusion, and the seasonal variation of water vapor content on the TP and surrounding areas was well represented in all datasets.

Table 2
Correlation coefficients, bias and RMSE of radiosonde data and each product on different time scales

		Annual	Spring	Summer	Autumn	Winter
AIRS-only	CC	0.94	0.96	0.88	0.94	0.97
	BIAS(mm)	-0.05	0.02	-0.07	-0.07	-0.02
	RMSE(mm)	2.38	1.74	4.58	2.79	1.13
ERA-5	CC	0.97	0.97	0.95	0.97	0.98
	BIAS(mm)	-0.04	0.09	-0.06	-0.04	-0.05
	RMSE(mm)	1.74	5.27	3.06	2.04	0.97
MERRA2	CC	0.96	0.97	0.93	0.96	0.98
	BIAS(mm)	0.04	0.05	0.05	0.02	-0.01
	RMSE(mm)	1.92	1.60	3.34	2.12	1.04
weighted ensemble data	CC	0.96	0.97	0.94	0.96	0.97
	BIAS(mm)	-0.01	0.02	-0.03	-0.03	-0.03
	RMSE(mm)	1.88	1.61	3.20	2.17	1.09

Spatiotemporal distribution of water vapor content

Spatial distribution characteristics of water vapor content

The spatial distribution of AIRS-only, ERA-5, MERRA2, and the weighted ensemble of annual water vapor content data over the TP and its surroundings from 2003–2019 are shown in Fig. 2. The spatial distribution of water vapor content was almost consistent across the four datasets, with the maximum value occurring in the southern part of the surroundings of the TP and decreasing deeper into the interior of the TP. Water vapor in the TP interior mainly comes from the lower latitudes. It enters through large canyons such as the Brahmaputra River, making it difficult for water vapor to enter the interior. There are two main moisture transport channels in the south, the Indian Ocean summer winds and the mid latitude westerly winds, which divide into two branches when they reach the western border of the TP. Water vapor content in north of the Tian shan is higher than in the TP's interior. Since most of the water vapor is active in the lower atmosphere, there is more water vapor at lower topographic heights. The north of the Tian

shan is at a lower elevation than the TP inland. The area north of the Tian shan has high water vapor content due to the lower elevation compared to the TP.

The spatial distribution of water vapor content in the TP and surrounding areas during the four seasons is shown in Fig. 3, which shows that the spatial distribution of water vapor content in the four seasons was roughly the same as the annual average water vapor content, forming a low-value region centered on the TP and a high-value region centered on the southern part of the surroundings of the TP. The maximum water vapor content occurred in summer due to the large amount of warm, moist water vapor brought by the summer winds from the lower latitudes (the Bay of Bengal and the Arabian Sea) northward[32]. As shown in Fig. 3a2–d2, the maximum moisture contents of AIRS-only, ERA-5, MERRA2, and weighted ensemble data in summer were 59.76 mm/day, 66.44 mm/day, 67.74 mm/day, and 64.62 mm/day, respectively. In winter, the TP and surrounding areas are mainly controlled by the prevailing westerly winds. The low atmospheric temperature over the plateau has limited capacity to hold water vapor, resulting in a dry atmosphere with minimum values below 1 mm/day (Fig. 3a4–d4). Water vapor content in spring and autumn was between that of summer and winter.

To assess the ability to capture the spatial distribution of water vapor content on the TP and surrounding areas, we used Fig. 2 to show the bias of the radiosonde stations from the reanalysis and satellite data. The biases of AIRS-only, ERA-5, MERRA2, and weighted ensemble data were unevenly distributed. In the Qilian Mountains and the Qaidam Basin, water vapor content was overestimated. At the same time, water vapor content was underestimated in the northern part of the Hengduan Mountains. At the Ejinnaqi station, the biases of AIRS-only, ERA-5, MERRA2, and weighted ensemble data reached maximum values of 0.48 mm, 0.35 mm, 0.5 mm and 0.44 mm, respectively, while at the Changdu station in the northwest of the Hengduan Mountains, these sets of data had the largest negative deviations at − 0.35 mm, − 0.28 mm, − 0.27 mm and −-0.3 mm respectively. It is worth noting that the bias of ERA-5 data was generally smaller than that of other sets of data. Almost all AIRS-only and MERRA2 data were similarly underestimated or overestimated. In the upper right corner of Fig. 2, the RMSE of each dataset and the radiosonde stations is shown, with the largest RMSE for AIRS-only (2.38 mm) and the smallest for ERA-5 (1.74 mm). In conclusion, all four datasets represented the spatial distribution of water vapor content on the TP and its surroundings well. The ERA-5 data had the best ability to reproduce the spatial distribution of the average water vapor content on the TP and surrounding areas.

Temporal characteristic of water vapor content

The temporal changes of atmospheric water vapor content on the TP and its surroundings from 1970 to 2019 are shown in Fig. 4. Guo *et al.*[33]and Hao *et al.*[34]showed that the radiosonde instruments in China changed in the early 2000s, resulting in large data changes. Since the radiosonde data had the highest correlation with the ERA-5 data, the ERA-5 data was used to calibrate the water vapor content from 2006 to 2019. From the annual scale, as shown in Fig. 4e, ERA-5, MERRA2, weighted ensemble and radiosonde data showed a significant increase trend, but the satellite product AIRS-only data did not show a similar trend due to the shorter time series. Several datasets had the same fluctuating trend as the radiosonde

stations and had higher water vapor content than the radiosonde data. The ERA-5, MERRA2, and AIRS-only dataset had a maximum water vapor contents of 17.17 mm/day, 16.15 mm/day, and 15.46 mm/day in 2016, respectively.

This paper also analyzed the temporal trends of the average water vapor content in the four seasons on the TP and surrounding areas, Except for the winter, the water vapor content in the other three seasons showed an increasing trend without significant changes as shown in Fig. 4. In the spring and autumn, the increasing trend of each product was not obvious. Compared with the spring, the increasing trend became especially obvious in the summer, with the maximum moisture content and a large fluctuation. The water vapor content in winter showed a constant or decreasing trend. Consistent with the annual average variation, each product's four seasons coincided with the fluctuating trend of the radiosonde data. The remaining products overestimated the seasonal average water vapor content relative to the radiosonde stations. The differences were largest in summer followed by spring and autumn and the smallest difference were in winter.

From the timescale, we found that the difference between ERA-5 data and the radiosonde data was the largest, and the AIRS-only was the smallest.

The relationship between water vapor content and precipitation and temperature

Under the background of global warming, the evaporation capacity of the earth's surface has significantly increased, and the air is able to hold more water vapor. As the material basis of precipitation generation, the water vapor content can directly affect precipitation weather and climate. Therefore, based on the spatial and temporal distribution of water vapor content on the TP and surrounding areas, we analyzed the relationship between temperature, precipitation and water vapor content in the region using calibrated TRMM precipitation data and ERA-5 temperature data. Figure 5 shows the spatial distribution of multiyear average temperature and precipitation on the TP and surrounding areas. As shown in Fig. 5a,a high precipitation value area was centered around the southeast part of the TP, where the maximum annual precipitation was more than 2500 mm. However, the precipitation within the TP was low, decreasing from southeast to northwest with the increase in elevation. The precipitation of Tarim Basin and Junggar Basin was less than 100 mm. These were the driest areas of TP and its surroundings. As shown in Fig. 5b, the temperature distribution on the plateau was closely related to the terrain. Temperatures on the plateau were generally cooler than those in the surroundings, with the highest temperatures occurring in the southwestern part of the TP surrounding areas, reaching over 25°C, while temperatures in the inner plateau ranged from − 10 to 8°C.

From the spatial distribution of temperature and precipitation on the TP and surrounding areas, it is clear that the spatial distribution was extremely uneven in this region. Therefore, it was necessary to study the temperature and precipitation characteristics and their relationship to water vapor content by zones. The

TP and surrounding areas are composed of 21 mountains, which were ordered and studied from west to east and from south to north. Figure 6 shows the distribution of water vapor content, temperature and precipitation, and the correlation between temperature, precipitation and water vapor content in the 21 mountains. On the whole, the water vapor content of the TP had a high correlation with temperature and precipitation at 0.88 and 0.72 respectively. The total annual water vapor content of the Himalaya, Kangri Garpo, and Hengduan Shan mountains in the southern part of the TP was higher than that of the other mountains, with values above 3700 mm/year. This was consistent with the distribution of water vapor content, precipitation, and temperature all of which were higher in these ranges than in the other ranges, except for West Himalaya, where precipitation was above 400 mm/year and temperature was above 4°C. This reflected the close correlation between precipitation, temperature and moisture content in the southern TP, indicating that the changing trends between the three variables were relatively consistent. The lowest water vapor content was found in Karakoram at 1279 mm/year. The temperature was also the lowest in this mountain range at only − 9.8℃. The lowest precipitation was found in Altun Shan at 58 mm/year. There was a good contrast between temperature and water vapor content in each mountain range, showing a significant positive correlation, while the relationship between precipitation and water vapor content varied in different mountains, indicating that the amount of precipitation in the various mountain ranges of the TP was influenced by many factors. There is no simple linear relationship between precipitation and water vapor content. The correlation between temperature and water vapor content is higher than 0.5 in all mountains except Nyainqentanglha and Tanggula Shan, and the highest correlation of 0.96 was found in Western Kunlun Shan. With increasing latitude, the correlation between precipitation and water vapor content decreased. The highest correlation appeared in Kangri Garpo, which it was as high as 0.98. The five mountains Western Kunlun Shan, Eastern Kunlun Shan, Eastern Tien Shan, Altun Shan, and Dzhungarsky Alatau were negatively correlated with water vapor content.

Overall, according to the Clausius-Clapeyron equation, increasing temperature makes the saturated water vapor pressure increase. The higher the temperature, the stronger the water holding capacity[35]. We found that areas with high temperatures on the TP had high water vapor content. This result was consistent with the above equation. However, precipitation is a complex process in which sufficient water vapor, dynamic uplift, and unstable energy are all necessary. From the above analysis, it was not difficult to see that the influence of water vapor content on the TP on precipitation varied with the region.

Conclusion And Discussion

This paper explored the following three questions using water vapor data and precipitation data from AIRS-only, TRMM, ERA-5, MERRA2, radiosonde stations, and V3.0. (1) What is the spatial and temporal distribution of water vapor content on the TP and surrounding areas? (2) What is the satellite and reanalysis data's ability to capture the water vapor content of the TP and its surroundings relative to the V3.0 measured data? (3) From the spatial distribution of precipitation and temperature, does the water vapor content of the TP and surrounding areas interact with precipitation and air temperature? The results indicated that:

Spatially, the high water vapor content areas were mainly located in the southern part of the Himalayas, the plateau's inner part was a low-value area, and the spatial distribution was very similar between years and seasons. Over time, the water vapor content has shown an increasing trend in the last 50 years, which was consistent with the background of global warming and humidification, and the seasonal differences were obvious, with the largest water vapor content value and increasing trend in summer, followed by spring and autumn, and the smallest in winter.

AIRS-only, MERRA2, ERA-5, and weighted ensemble data could capture the spatial and temporal distribution of water vapor content on the TP and the surrounding areas. Spatially, the ERA-5 data had the highest correlation with the lowest RMSE, indicating that it was the best in assessing the annual and seasonal spatial distribution of water vapor content on the TP and its surroundings. Over time, the four sets of products' fluctuation trend was basically consistent with the radiosonde stations, the water vapor content was higher than the radiosonde stations, and the weighted ensemble data showed good integration.

The southern and southeastern regions surrounding the TP formed a high precipitation zone, and precipitation within the plateau showed a decreasing trend from southeast to northwest. The correlation between precipitation and water vapor content was highest in the southern part of the TP and decreased with increasing latitude. Temperature in the southern and southwestern regions surrounding the TP formed a high precipitation zone, and temperature within the plateau gradually decreased with increasing altitude, while air temperature and water vapor content on the TP showed a significant positive correlation, indicating a close relationship.

Water vapor on the TP and surrounding areas plays an important role in the global water cycle. This paper used multisource data to analyze the spatial and temporal variation of water vapor content and the spatial distribution of precipitation conversion rates in the region, which not only made the conclusions more reliable but also compared the ability of the above data sources to capture the water vapor content of the TP and surrounding areas. It is hoped that this paper will help in the study of the water cycle and the rational and efficient development of aerial water resources on the TP and surrounding areas. However, this paper lacks a discussion of the sources and transport processes of water vapor on the TP and surrounding areas on different time scales. More comprehensive data are needed to make the results more generalizable in the future.

Declarations

Acknowledgments

This work was supported by the National Natural Science Foundation of China (41801052 and 41861013)

Author Contributions

M.S. and X.Y. designed the research Z.W. and L.Z. and H.Z. collected the data Z.W. wrote the manuscript and prepared all figures. All authors discussed the results and reviewed the manuscript.

Additional Information

Competing Interests: The authors declare no competing interests.

Publisher's note: Springer Nature remains neutral with regard to jurisdictional claims in published maps and institutional afliations.

References

1. Varamesh, S., Hosseini, S. M. & Rahimzadegan, M. Estimation of atmospheric water vapor using MODIS data 1. (case study: Golestan province of Iran). *J Mater Environ Sin.* **8**, 1690–1695 (2017).
2. Liu, G. W. The atmospheric process of the hydrologic cycle.*Beijing: China Science Press.*25–56(1997).
3. Zhang, Q., Zhang, J. & Sun, G. W. & Di X.H. Research on atmospheric water-vapor distribution over Qilianshan mountains. *Acta Meteor Sinica.* **65**, 633–643 (2007).
4. Zhou, T. J., Gao, J., Zhao, Y., Zhang, L. X. & Zhang, W. X. Water Vapor Transport Processes on Asian Water Tower. *Bull Chin academy sci.* **34**, 1210–1219 (2019).
5. Yang, Q., Liu, X. Y., Cui, C. X., Li, J. & Liu, R. The computation and characteristics analysis of water vapor contents in the Tarim Basin, China. *Acta Geogr Sin.* **65**, 853–862 (2010).
6. Wang, A. H. & Zeng, X. B. Evaluation of multireanalysis products with in situ observations over the Tibetan Plateau. *J Geophys Res Atmos.* **117**, 214–221 (2012).
7. Liu, J. J., You, Q. L. & Wang, N. Interannual anomaly of cloud water content and its connection with water vapor transport over the Tibetan Plateau in summer. *Plateau Meteor.* **38**, 449–459 (2019).
8. Zhu, B., Zhang, Q., Lu, G. Y., Li, D. H. & Li, C. H. Analysis of the distribution characteristics and trend of air vapor in Qilian Mountains. *Plateau Meteor.* **38**, 935–943 (2019).
9. Chen, D., Zhou, C. Y. & Deng, M. Y. A comparison analysis of three reanalysis datasets in the change of atmospheric water vapor content in the summer of the Tibetan Plateau. *Plateau Mountain Meteor*

Res. **38**, 1–6 (2018).

10. Zhang, Y. W., Wang, D. H., Zhai, P. M., Gu, G. J. & He, J. H. Spatial distributions and seasonal variations of tropospheric water vapor content over the Tibetan Plateau. *J Clim.* **26**, 5637–5654 (2013).
11. Zhuo, G., Bian, B. C. R., Yang, X. H. & Luo, B. Spatial and temporal changes of atmospheric precipitable water in Tibet Region in recent 30 years. *Plateau Meteor.* **32**, 23–30 (2013).
12. Lin, H. B., You, Q. L., Jiao, Y. & Min, J. Z. Water vapor transportation and its influences on precipitation in summer over Qinghai-Xizang Plateau. *Plateau Meteor.* **35**, 309–317 (2016).
13. Han, Y. Z., Ma, W. Q., Wang, B. Y. & Ma, Y. M. Climatic characteristics of rainfall change over the Qinghai-Tibetan Plateau from 1980 to 2013. *Plateau Meteor.* **36**, 1477–1486 (2017).
14. Yao, J. Q. *et al.* Characteristics analysis of water vapor contents around Tianshan Mountains and the relationships with climate factors. Tianshan Mountains and the Relationships with Climate. *Sci Geogr Sin.* **33**, 859–864 (2013).
15. Zhou, S. W., Wu, P., Wang, C. H. & Han, J. C. Spatial distribution of atmospheric water vapor and its relationship with precipitation in summer over the Tibetan Plateau. *J Geogr Sci.* **22**, 795–809 (2012).
16. Xie, H., Ye, J. S., Liu, X. M. & E, C. Y. Warming and drying trends on the Tibetan Plateau (1971–2005). *Theor Appl Climatol.* **101**, 241–253 (2010).
17. Cess, R. D. Water vapor feedback in climate models. *Science.* **310**, 795–796 (2005).
18. Li, W., Liu, J. C., Shang, B. & Xu, C. Analysis on the relationship between atmospheric water vapor content and temperature and precipitation in Changchun. *Meteorological disaster prevention.* **26**, 6–9 (2019).
19. Yao, Y. B. *et al.* Analysis of precipitable water vapor and surface temperature variation over Qinghai-Tibetan Plateau from 1979 to 2014. *Chin Sci Bull.* **61**, 1462–1477 (2016).
20. Xiong, C., Yao, R. Z., Shi, J. C. & Lei, Y. H. Change of snow and ice melting time in High Mountain Asia. *Chin Sci Bull.* **64**, 2885–2893 (2019).
21. Yao, T. D., Thompson, L. & Yang, W. Different glacier statusw with atmospheric circulations in Tibetan Plateau and surroundings. *Nat Clim Change.* **2**, 663–667 (2012).
22. Xie, Z. C., Zhou, Z. G., Li, Q. Y. & Wang, S. H. Progress and prospects of mass balance characteristic and responding to global change of glacier system in High Asia. *Adv Earth Sci.* **24**, 1065–1072 (2009).
23. Wang, S. J. *et al.* Recent changes in freezing level heights in High Asia and their impact on glacier changes. *J Geophys Res: Atmos.* **119**, 1753–1765 (2014).
24. Xu, B. R. *et al.* Variation of tropospheric specific humidity upon the middle-lower reaches of the Heihe River during 1981–2010. *Journal of Glaciology and Geocryology.* **38**, 57–68 (2016).
25. Chahine, M. T., Pagano, T. S., Aumann, H. H., Atlas, R. & Granger, S. AIRS: improving weather forecasting and providing new data on greenhouse gases. *Bull amer meteor soc.* **87**, 911–926 (2006).

26. Zhao, Y. & Zhou, T. J. Asian water tower evinced in total column water vapor: a comparison among multiple satellite and reanalysis data sets. *Clim Dynam.* **54**, 231–245 (2020).
27. Kummerow, C., Barnes, W. & Kozu, T. The tropical rainfall measuring mission (TRMM) sensor package. *J Atmos Ocean Technol.* **15**, 809–817 (1998).
28. Zhao, L., An, S. Z., Yang, L. M., Ma, Y. F. & Zhang, G. X. Study on Precipitable Water and Precipitation Conversion Efficiency in Urumqi during the Period of 1976–2007. *Arid Zone Research.* **27**, 433–437 (2019).
29. Lu, N. *et al.* Trends and variability in atmospheric precipitable water over the Tibetan Plateau for 2000–2010. *Int J Climatol.* **35**, 1394–1404 (2015).
30. Molod, A., Takacs, L., Suarez, M. & Bacmeister, J. Development of the GEOS-5 atmospheric general circulation model: evolution from MERRA to MERRA2. *Geosci Model Dev.* **7**, 339–1356 (2015).
31. Wang, B. Z. & Liu, G. S. An estimation of total atmospheric water vapor in the mainland of China. *Acta Geogr Sin.* **48**, 244–253 (1993).
32. Feng, L. & Zhou, T. J. Water vapor transport for summer precipitation over the Tibetan Plateau: Multidata set analysis. *J Geophys Res.* **117**, D20114 (2012).
33. Guo, Q. Y., Zhao, P. T., Zhang, Y. C. & Liu, F. Q. Technical improvement and experimental analysis of GTS1 radiosonde. *Meteor Sci Technol.* **41**, 254–258 (2013).
34. Hao, M., Gong, J. D., Wang, R. W., Wan, X. M. & Liu, Y. The quality assessment and correction of the radiosonde humidity data biases of L-band in China. *Acta Meteor Sinica.* **73**, 187–199 (2015).
35. Liang, H. Variation of the atmospheric water vapor and its radiative effect simulations over the Tibetan Plateau. Doctor Dissertation. Beijing: Chin Academy Meteor Sci.(2012).

Figures

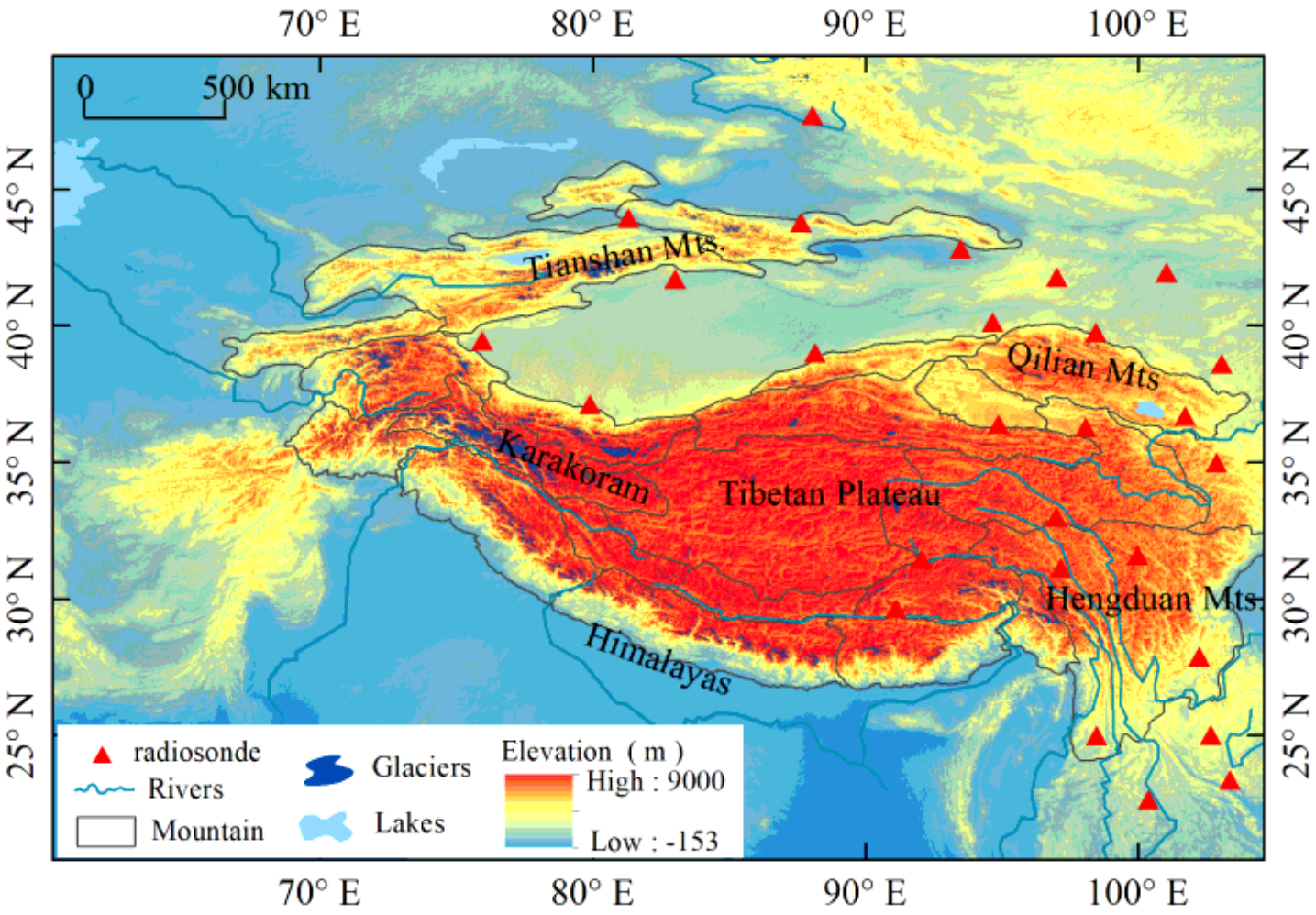

Figure 1

Location of the study region. Note: The designations employed and the presentation of the material on this map do not imply the expression of any opinion whatsoever on the part of Research Square concerning the legal status of any country, territory, city or area or of its authorities, or concerning the delimitation of its frontiers or boundaries. This map has been provided by the authors.

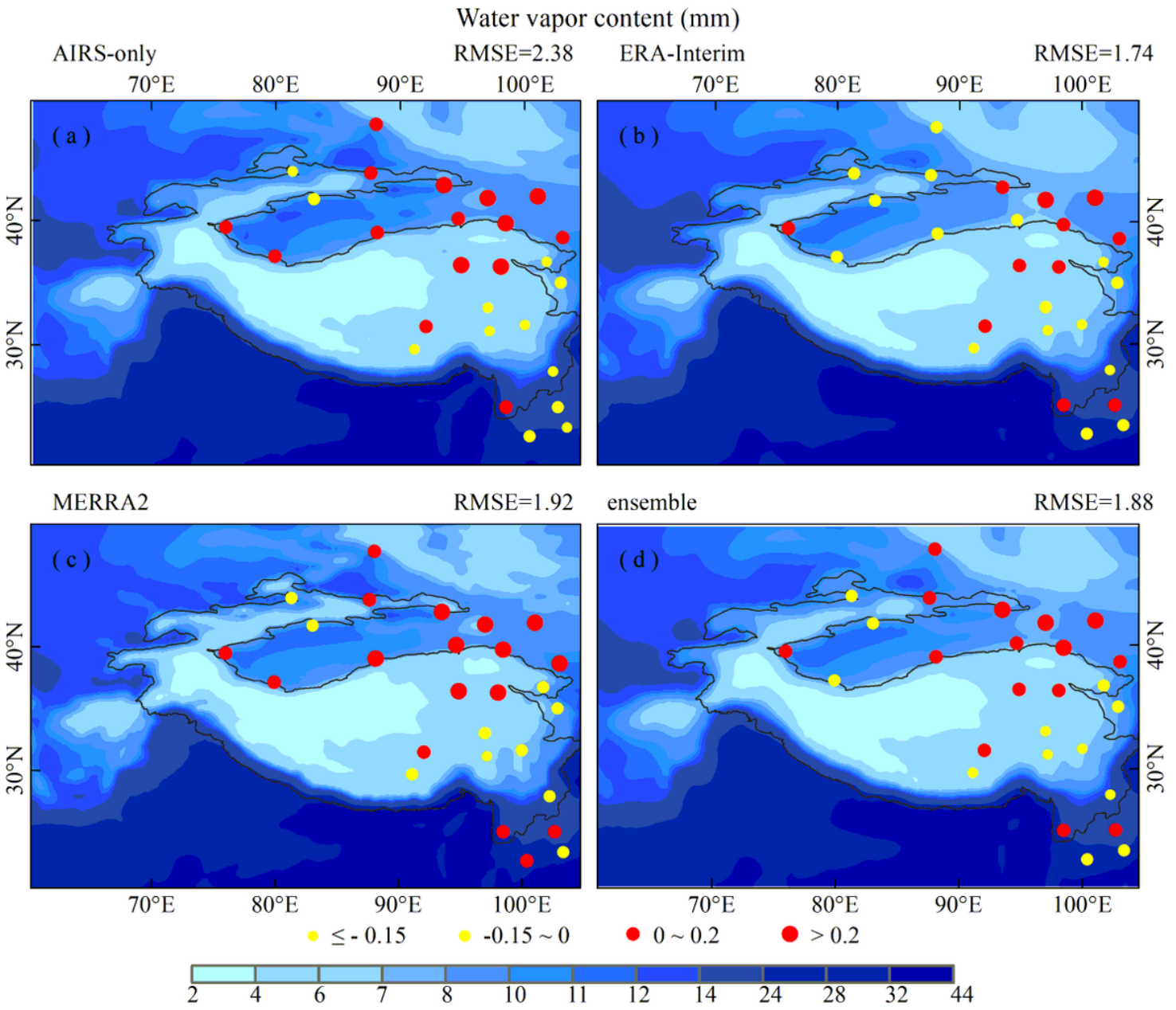

Figure 2

AIRS- only, ERA-5, MERRA2 and ensemble data on diurnal variation of the water vapor of the Tibetan Plateau and surrounding areas from 2003 to 2019Dots and related numbers represent biases compared to radiosonde dataset, red dots denote positive biases, and yellow dots denote negative biases, their RMSE values are printed on the top-right of each panel). Note: The designations employed and the presentation of the material on this map do not imply the expression of any opinion whatsoever on the part of Research Square concerning the legal status of any country, territory, city or area or of its authorities, or concerning the delimitation of its frontiers or boundaries. This map has been provided by the authors.

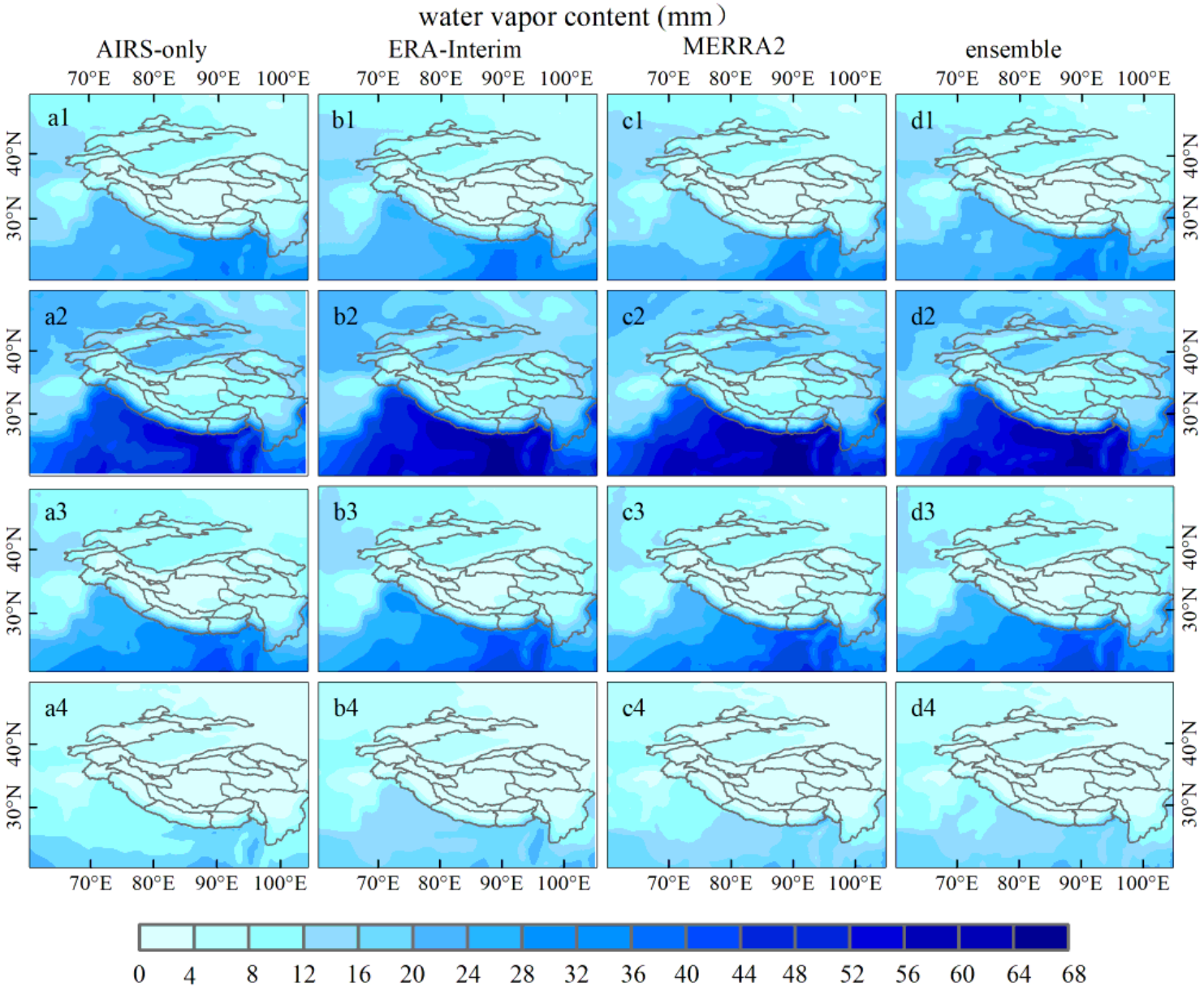

Figure 3

AIRS- only, ERA-5, MERRA2 and ensemble data on the spatial distribution of water vapor content on the Tibetan Plateau and surrounding areas in four seasons from 2003 to 2019（spring (a1 – d1), summer (a2 –d2), autumn (a3 – d3) and winter (a4 – d4)). Note: The designations employed and the presentation of the material on this map do not imply the expression of any opinion whatsoever on the part of Research Square concerning the legal status of any country, territory, city or area or of its authorities, or concerning the delimitation of its frontiers or boundaries. This map has been provided by the authors.

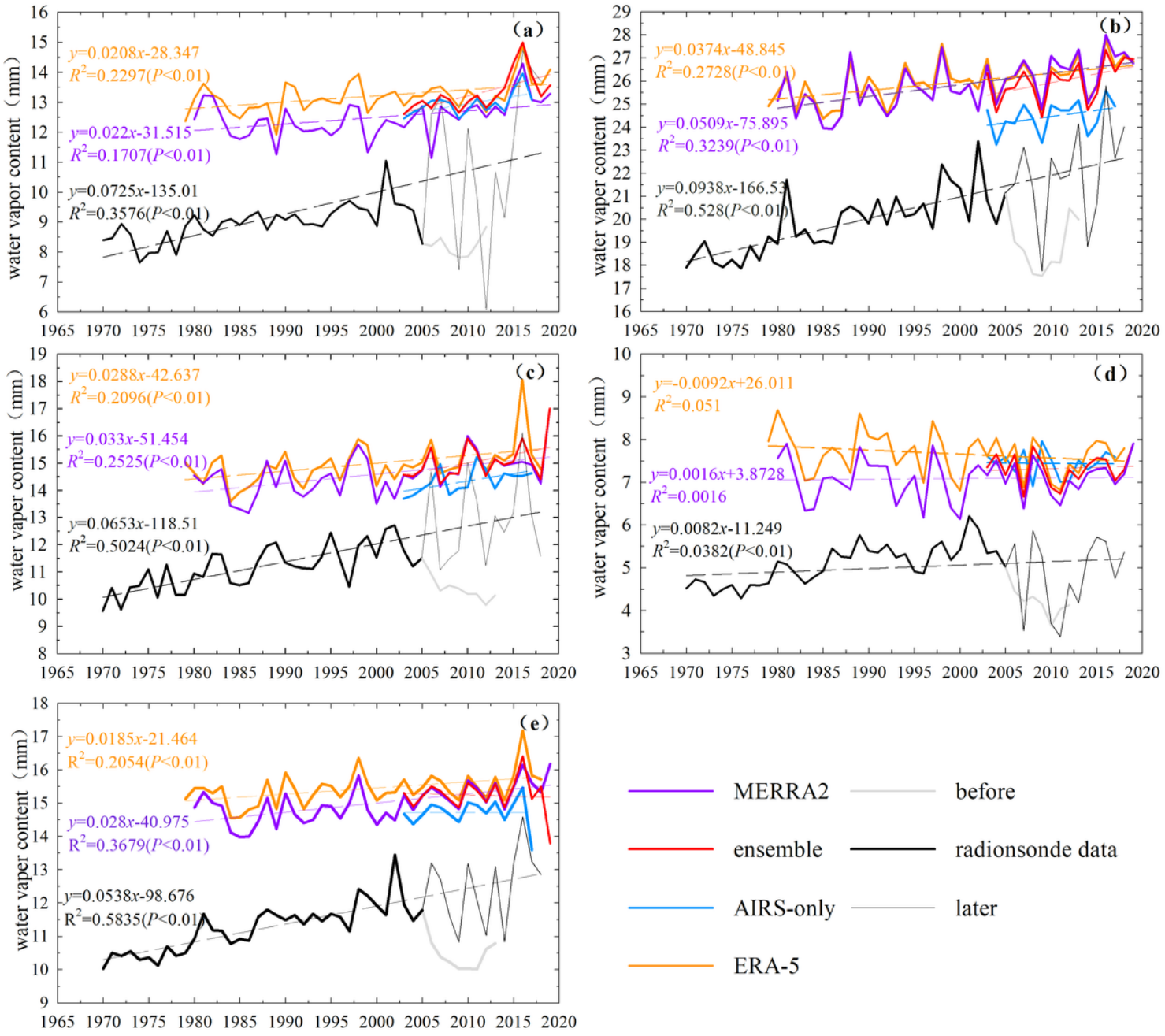

Figure 4

Seasonal changes of water vapor content between AIRS-only, ERA-5, MERRA2, weighted ensemble, and radiosonde data in the TP and surrounding areas for the period of 1970–2019.(a) spring, (b) summer, (c) autumn, (d) winter, and (e) annual

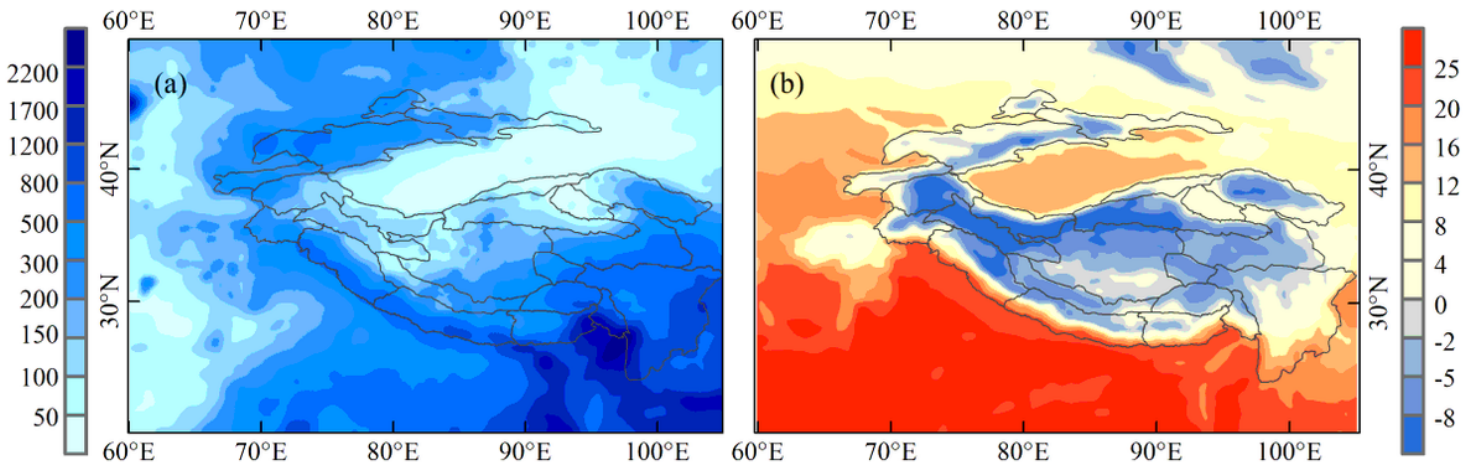

Figure 5

The spatial distribution of precipitation (a) and temperature (b) in the TP and surrounding areas from 2003 to 2019. Note: The designations employed and the presentation of the material on this map do not imply the expression of any opinion whatsoever on the part of Research Square concerning the legal status of any country, territory, city or area or of its authorities, or concerning the delimitation of its frontiers or boundaries. This map has been provided by the authors.

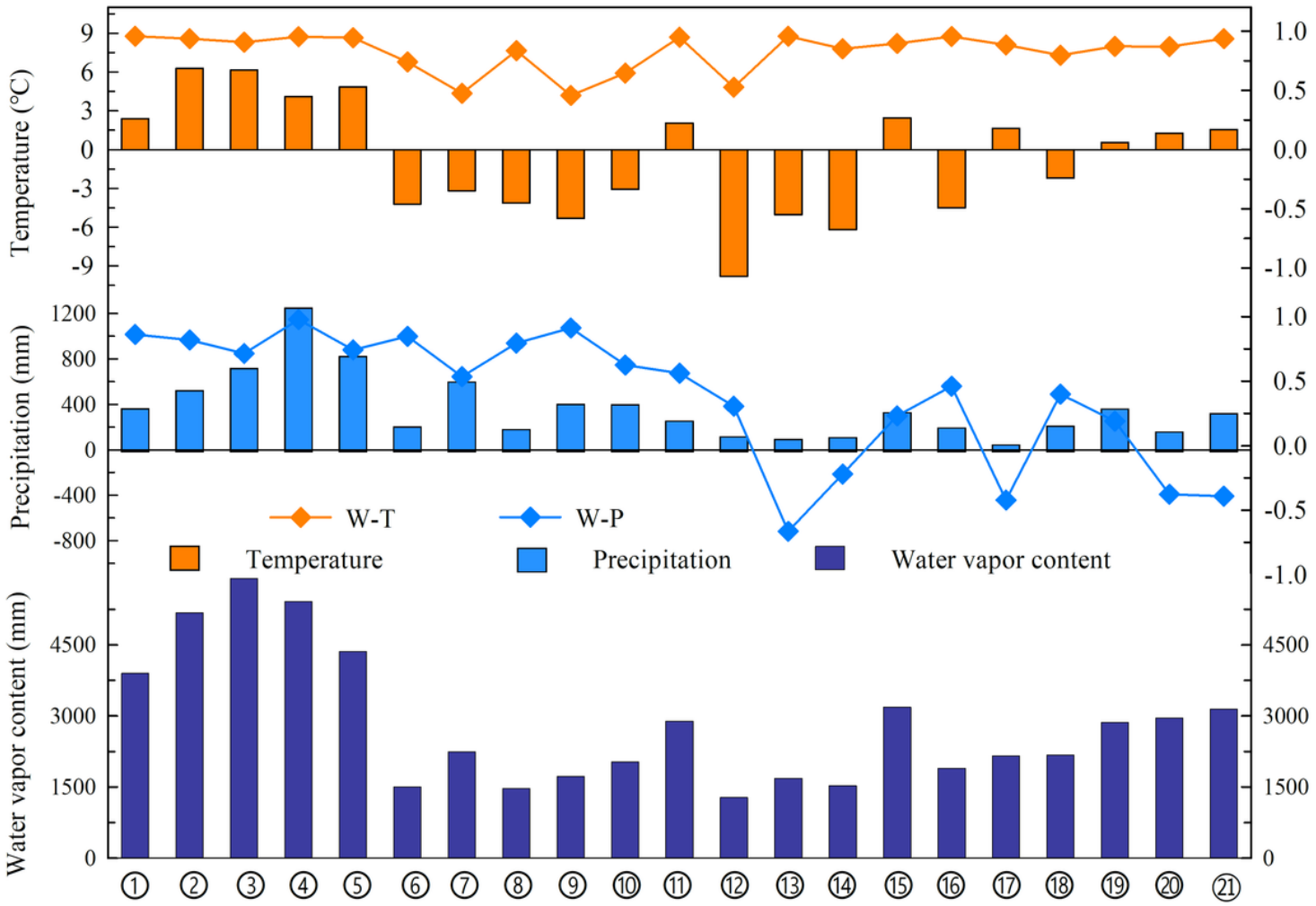

Figure 6

The distribution of water vapor, temperature, and precipitation in 21 main mountain ranges on the TP and surrounding areas from 2003 to 2019, analyzing the correlation between water vapor and temperature and precipitation (①West Himalaya ②Central Himalaya ③East Himalaya ④Kangri Garpo ⑤Hengduan Shan ⑥Gangdise Mountains ⑦Nyainqentanglha ⑧Tibetan Interior Mountains ⑨Tanggula Shan ⑩Eastern Tibetan Mountains ⑪East Hindu Kush ⑫Karakoram ⑬Western Kunlun Shan ⑭Eastern Kunlun Shan ⑮Pamir Alay ⑯Pamir &Altun Shan ⑰Qilian Shan ⑱Central Tian Shan ⑲Western Tian Shan ⑳Eastern Tian Shan ㉑ Dzhungarsky Alatau)